17th Australasian Fluid Mechanics Conference
Auckland, New Zealand
5-9 December 2010

Experimental and Computational Analysis of a Transonic Compressor Rotor

A. Boretti[1]

[1]School of Science and Engineering,
University of Ballarat, Ballarat, Victoria 3353, Australia

Abstract

Assessment of computational fluid dynamic (CFD) codes used for the design and analysis of turbo machinery is a subject covered by many researchers. NASA Rotor 37 is one of the most used transonic compressor test cases. In a blind test case conducted by ASME and IGTI, and for a subsequent test case conducted by AGARD, most of the participating codes over predicted pressure and temperature ratios, and failed to predict certain features of the downstream flow field. These days, this test case is still an important assessment of industrial and research CFD codes. In this work, STAR-CCM+ is used to predict the transonic compressor flows. The turbulence is represented through a RANS model with the SST (Menter) k-ω variant and the all y+ wall treatment. Comparisons are made with overall performance maps and span wise profiles of aerodynamic parameters. Results obtained are in good agreement with the experimental data although there are still some important discrepancies.

NASA Rotor 37

NASA Rotor 37 is one of the most used transonic compressor test cases. Rotor 37 is a low aspect ratio inlet rotor for a core compressor. It was originally tested as a stage by Reid and Moore in 1978 and 1980 [1 and 2]. The rotor was re-tested at NASA Glenn by Suder et al. in 1994 [4] and more recently by Shabbir et al. in 1997 [12]. Radial distributions of static and total pressure, total temperature, and flow angle as well as detailed laser anemometry measurements of the velocity field within the rotor and wake were used for a blind test case conducted by ASME and IGTI, and for a subsequent test case conducted by AGARD in 1994-1998 [3]. Most of the participating codes over predicted pressure and temperature ratios, and failed to predict certain features of the downstream flow field. These days, this test case is still an important assessment of industrial and research CFD codes [5-11]. In this work, STAR-CCM+ [13] is used to predict the transonic compressor flows with different models for turbulence and different levels of grid refinement.

Rotor 37 was designed and initially tested as part of a research programme involving four related axial-flow compressor stages intended to cover a range of design parameters typical of aircraft turbine engine high-pressure (core) compressor inlet stages. In the case of stage 37, representative values were:

- Rotor inlet hub-to-tip diameter ratio 0.7;
- Rotor blade aspect ratio 1.19;
- Rotor tip relative inlet Mach number 1.48;
- Rotor hub relative inlet Mach number 1.13;
- Rotor tip solidity 1.29;
- Blade airfoil sections Multiple-Circular-Arc (MCA).

No inlet guide vanes were specified for any of the stages. First overall stage performance results were reported by Reid and Moore, 1978 [1]. More detailed stage performance was reported later by Moore and Reid, 1980 [2]. It should be noted that while the designs and stage tests were initiated during the 197O's, geometries and performance levels are similar to those for current turbine engine stages. Design point values for the rotor as estimated in the design computations were (T_{0l} = inlet total temperature, T_{ref}= 288.15 K sea level standard temperature, p_{01} inlet total pressure, p_{ref} =101.33 kN/m^2 sea level standard pressure, A_a = annulus area):

- Equivalent rotational speed $N \cdot (T_{ref}/T01)^{1/2}$= 17188.7 rpm (1800 rad/s);
- Equivalent rotor tip speed $U_t \cdot (T_{ref}/T_{01})^{1/2}$=454.1 m/s;
- Equivalent mass flow per unit annular area $MFR/A_a \cdot p_{ref}/p_{01} \cdot (T_{01}/T_{ref})^{1/2}$=200.5 kg/s/m^2;
- Rotor total pressure ratio = 2.106;
- Rotor polytrophic efficiency = 0.889;
- Number of rotor blades = 36.

Subsequent to the tests of Moore and Reid, 1980 [2] on NASA Stage 37, the rotor was retested as an isolated component. This is the geometry identified by NASA as Rotor 37.

Radial distributions of static and total pressure, total temperature, and flow angle were measured at two axial stations located 4.19 cm upstream and 10.67 cm downstream of the blade hub leading edge, labelled stations 1 and 4 respectively in Figure 1. Detailed laser anemometry measurements were made of the velocity field within the rotor and wake at several axial stations and on five span wise planes also shown in Figure 1. The Figure also shows the annular flow path and blade airfoil geometries with coordinate reference definitions for computational purposes. These coordinate definitions are those utilized in all data reported and in all performance computations reported. Additional geometric data of interest for CFD purposes, the blade hub fillet radius was 2.5 mm and the RMS blade surface roughness is 0.5 - 1.25 microns. The tip clearance is 0.0356 cm. The data sets selected for the WG26 code evaluation [4] included averaged overall performance values, rotor entrance and exit (Stations 1 and 4) probe survey information and selected laser anemometer results. The inlet station 1 is z=-4.19 cm, while the exit station 4 is z=+10.0 cm. The hub only rotates between z =0.246 and z = 4.521 cm. The rotor hub leading edge is at z = 0.

Inlet and outlet boundary conditions for CFD Codes should be defined on the basis of the results presented in Table 1, where p_0 and T_0 are absolute total pressure and temperature and η is the adiabatic efficiency. Inlet total pressure is 1 bar and inlet total temperature is 300 K. In addition, the turbulence intensity at station 1 is 3% while the hub and tip boundary layers are about 0.82 cm. The blade coordinates at different sections are presented in [1].

Experimental data show large dip in total pressure distribution near the hub at downstream of the rotor. Many researchers have tried to model rotor 37 by now, and no one quite gets it right. Some of them suggest this is because the casing boundary layer separates and the turbulence models don't do a very good job. Reference [3] covers a lot of the older papers. Most original numerical solutions from the blind test exercise did not predict this total pressure deficit correctly.

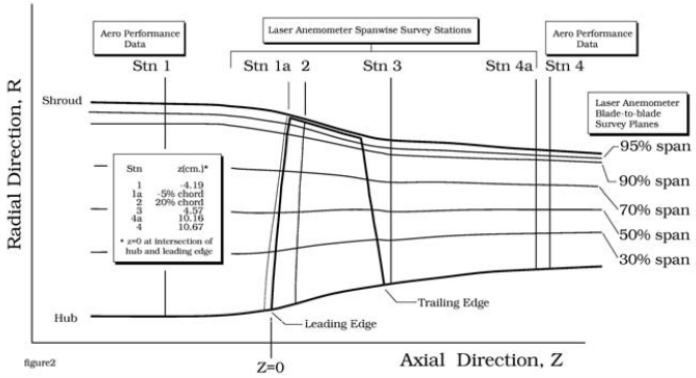

Figure 1 – Rotor 37 flow path from Chima (2009) [8]

Because of the poor performances of many CFD codes, the Rotor 37 test case was disqualified after a small hub leakage flow was identified by Shabbir, et al., 1997 [12]. As properly reported in [7], several subsequent numerical studies with different turbulence closure model properly calculated this dip in total pressure rise, even if several other studies failing the prediction also attributed this total pressure deficit to the small leakage flow. As the experimental study cannot be repeated, either explanation cannot be validated. It is however the opinion of the author as well as of others (Chima, 2009) [8] that the hub leakage effect is not a problem, it does not require modelling, and the test case is a accurate one, suitable for testing the capabilities of CFD codes.

MFR [kg/s]	MFR/ MFR*	p_{04}/p_{01}	η	T_{04}/T_{01}	
20.8798	1.0000	1.995	0.890	1.2451	Choked
20.8290	0.9976	1.992	0.889	1.2448	
20.8113	0.9968	2.018	0.891	1.2493	
20.6652	0.9897	2.065	0.887	1.2595	
20.5568	0.9845	2.071	0.879	1.2630	
20.5196	0.9828	2.084	0.879	1.2656	Near peak eff.
20.2348	0.9691	2.099	0.872	1.2706	
20.1345	0.9643	2.110	0.875	1.2718	
20.0579	0.9606	2.114	0.868	1.2747	
19.8084	0.9487	2.128	0.861	1.2797	
19.8052	0.9485	2.135	0.862	1.2807	
19.4092	0.9296	2.141	0.850	1.2858	
19.3897	0.9286	2.144	0.848	1.2871	Near stall

Table 1 – Rotor 37 blind test case operating curve

Details of set up for simulations

In this work, STAR-CCM+ [13] was used to predict transonic compressor flows. STAR-CCM+ [13] includes all the popular variants of k-ε (Standard, V2F, Realizable, Two-layer), k-ω (Standard, SST and BSL), Reynolds Stress (RSM - linear and quadratic), and Spalart-Allmaras Reynolds Averaged Navier Stokes (RANS) Turbulence models with different near-wall options, including Hybrid Wall Functions and Low and High Reynolds Number variants. The results for rotor 37 are very sensitive to turbulence model parameters. However, none of the models above is expected to provide a very accurate description of all the relevant physical phenomena.

The computational domain is made up of one blade passage delimited by inlet, exit, hub, tip and left and right periodic boundaries. Comparisons are made with overall performance maps and span wise profiles of several aerodynamic parameters. Adopted boundary conditions are stagnation or mass flow inlet, pressure outlet with radial equilibrium, no slip walls fixed or rotating, and cyclic.

Some researcher modify the inlet profiles of stagnation pressure or mass flow to account for turbulent boundary layers of same size on the hub and casing, estimated to be about 0.82 cm. This is also done for the results presented. The inlet flow direction is axial. Some researcher set the inlet radial flow angle to follow the grid, but this option is not considered here. The inlet Mach number cannot be set for internal flows. The mass flow depends directly on the exit static pressure, just like the flow through a C-D nozzle. Most researchers set the exit hub static pressure and solve radial equilibrium at the exit to get p(r) then monotonically increasing behind a rotor and not constant. This is also the option adopted here. Assuming stagnation inlet boundary conditions, most researchers extrapolate something to the inlet, usually a characteristic variable to complete boundary data, but the axial velocity component also may work fine. Eventually the solution converges with a mass flow that depends uniquely on the outlet pressure that may differ from the measured value. The flow can even be choked, in which case the shock location in the rotor depends on the outlet pressure. Usually the mass flow is not what is wanted, so $p_{4,hub}$ has to be redefined and the computation rerun until acceptable convergence.

We considered near peak efficiency and near stall operating points. For both cases the peak efficiency data is at 98-99% of the maximum mass flow. Table 2 summarizes the data measured and used as boundary conditions for the rotor37 simulations.

	Experimental		Computational	
% span	$p_{4,hub}/p_{01}$	MFR [kg/s]	$P_{4,hub}/p_{01}$	MFR [kg/s]
Choke	1.10	20.930	<1.1	20.930
Near Peak eff.	1.20	20.511	1.225	20.342
Near stall	1.25	19.360	1.286	19.510
Stall	-	19.235	-	-

Table 2 – Inlet and Outlet flow conditions set-up

The hub only rotates between z = -0.246 and z = 4.521 cm. The rotor hub leading edge is at z=0. Some researchers believe that air leaks into the flow path through the upstream gap between the stationary and rotating hub, and that this creates the low total pressures in the downstream profiles below 30% span [12]. As previously stated, the author doesn't believe that this is a problem and does not try to model this effect. The tip clearance is less than 0.04 cm (about 0.2 percent span) and it is accounted. The upstream and downstream gaps between the stationary and rotating hub are small and are neglected. Boundary condition along the hub surface is assumed to be no slip wall, fixed or rotating. Boundary condition along the shroud surface is also no slip wall fixed. No slip rotating wall boundary conditions are used along the blade surfaces. Periodic boundary conditions apply half the blade passage.

Selected results of computations

For the results presented hereafter, the grid was made up of 816,638 cells, with 2,412,630 faces and 856,112 verts. This grid refinement is about 3 times finer than the grids recommended by Dunham, et al. in [4]. The grid spacing at the blade and end walls is 4×10^{-4} cm, giving y^+ = 2 to 4 at the first grid point off the walls. In the tip clearance gap 13 points were used across the gap of 0.04 cm. The turbulence is represented through a RANS model with the SST (Menter) k-ω variant and the all y+ wall treatment.

The All y+ wall treatment is a hybrid model that attempts to provide a more realistic modelling than either the low-Re or the high-Re treatments for when the wall-cell centroid falls in the buffer region. It is a design goal that this wall treatment should give results similar to the low-y^+ treatment as $y^+\rightarrow0$ and to the high-Re treatment for $y^+>30$. Damping functions are used for the

source terms in the transport equation, but the model's source terms in the wall cell are suitably modified using the blended wall laws. This wall treatment is recommended for most simulations. The blended wall laws are intended to represent the buffer layer by appropriately blending the viscous sub-layer and logarithmic regions. For momentum, Reichardt's law [15] is used. For temperature, Kader's law [16] is used slightly modified for the effects of wall roughness.

Figure 2 – Details of hub (bottom), blade-to-blade mid span (mid) and shroud (top) computational grids

Figure 2 presents a view of the computational grid on the hub, blade-to-blade mid span and shroud planes. This picture shows the geometry of the blade in these sections. Figure 3 presents the computed and measure total temperature and total pressure ratios for operation near peak efficiency and near stall. These computational results show a satisfactory agreement with experiments despite differences are much larger than those typically found simulating the flow within other turbo machinery blades.

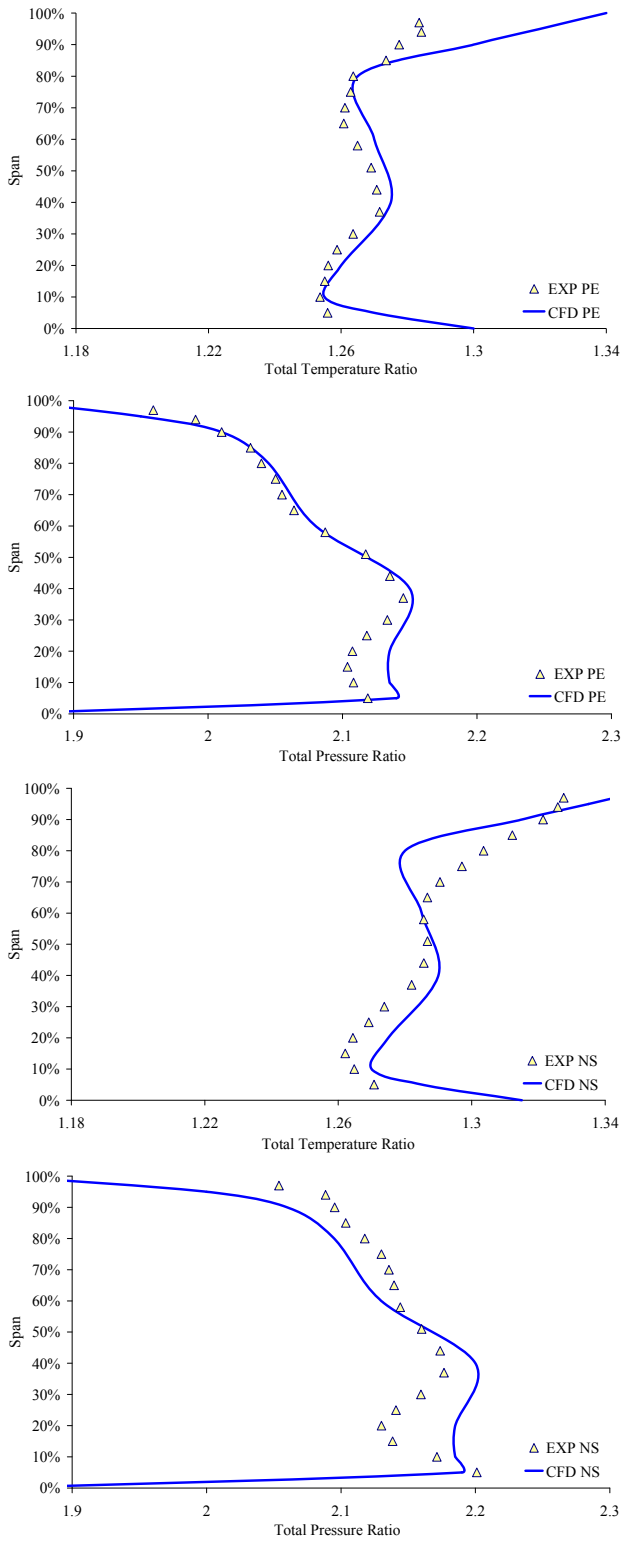

Figure 3 – Total temperature and total pressure ratio measured (EXP) and computed (CFD) for operation near peak efficiency (PE) and near stall (NS).

Simulations performed with different grids and different turbulence models - details not presented here because of the limited space available - show the RANS model of turbulence with the SST (Menter) k-ω variant and the all y+ wall treatment is the one that provide the best compromise between accuracy of results, computational effort (memory requirements and computational time) and grid independence of results.

Conclusions

The STAR-CCM+ [13] code was used to predict the performance of NASA rotor 37 transonic compressors. Relatively fine computational grids were used with 0.9 million points and 12 cells across clearance gaps. The RANS model of turbulence with the SST (Menter) k-ω variant and the all y+ wall treatment was used for all cases. There were areas where the code did not agree with the data.

Predicted exit total pressures below 40% span did not match the "deficit" seen in the data. This feature of the flow field seems to be intrinsic to the rotor design but could also be related to hub leakage in the experiment as suggested by Shabbir et al. [12].

Predicted exit total temperatures were high near the casing. This discrepancy was also seen in all of the results published in the AGARD report [3]. Probe measurements of total temperature were consistent with temperatures computed from laser anemometry data, so the experimental data appears to be correct.

On the casing the passage shock and clearance vortex meet up and cause the casing boundary layer to separate. The aft camber of the blade increases the adverse pressure gradient and the strength of the clearance flow that make the separation large. The predicted separation is probably too large as may be guessed from the over prediction of total temperature downstream.

The fact that all codes in the AGARD test case [3] over predicted total temperature near the casing suggests that no codes do well for the shock/vortex/boundary layer interaction close to the case. Unfortunately there is no good experimental data in this region, because probe and laser data both stop just below the separated region at 95% span.

Additional measurements in the separated region would be extremely useful for finally explaining this rotor, for improving CFD codes for highly loaded blades, and ultimately for designing rotors with better performance near the casing.

STAR-CCM+ offers the advantage to solve computational fluid dynamic problems exploring almost all the options available for physics and grids with the simplicity of a few clicks of mouse. STAR-CCM+ permits almost anyone to make his/her own judgement on the influence physic and grid refinement may have on the computational results.

What makes a CFD tool practically usable is not the ability to solve the more complicated physical models or the adoption of the smallest possible time and space discretization scales, but the extensive validation performed versus good experimental results. Only validation versus reliable experiments enables replacement of some of these experiments with simulations. The best quality a CFD specialist must have is the ability to perform and understand experiments.

References

1. Reid, L., and Moore, R. D., "*Design and Overall Performance of Four Highly-Loaded, High-Speed Inlet Stages for an Advanced, High-Pressure-Ratio Core Compressor*", NASA TP-1337, 1978. http://ntrs.nasa.gov/archive/nasa/casi.ntrs.nasa.gov/19780025165_1978025165.pdf
2. Reid, L., and Moore, R. D., "*Experimental Study of Low Aspect Ratio Compressor Blading*", ASME Paper 80-GT-6, March 1980.
3. AGARD-AR-355, "*CFD Validation for Propulsion System Components*", January 1998. ISBN 92-836-1075-X / NASA-19980203585. http://ftp.rta.nato.int/public//PubFullText/AGARD/AR/AGARD-AR-355///AGARD-AR-355.pdf
4. Suder, K.L., and Celestina, M.L., "*Experimental and computational investigation of the tip clearance flow in a transonic axial compressor rotor*", NASA-TM-106711, 1995. http://ntrs.nasa.gov/archive/nasa/casi.ntrs.nasa.gov/19950025317_1995125317.pdf
5. Chima, Rodrick V., "*Calculation of Tip Clearance Effects in a Transonic Compressor Rotor*", NASA TM-107216, 1996. Also ASME Paper 96-GT-114, June 1996. http://ntrs.nasa.gov/archive/nasa/casi.ntrs.nasa.gov/19960026671_1996059092.pdf
6. Chima, Rodrick V., and Liou, M.S., "*Comparison of the AUSM+ and H-CUSP Schemes for Turbomachinery Applications*", NASA TM-2003-212457, 2003. Also AIAA Paper 2003-4120. http://ntrs.nasa.gov/archive/nasa/casi.ntrs.nasa.gov/20030063293_2003072678.pdf
7. Hah, C., "*Large Eddy Simulation of Transonic Flow Field in NASA Rotor 37*", NASA/TM-2009-215627, 2009. http://ntrs.nasa.gov/archive/nasa/casi.ntrs.nasa.gov/20090038700_2009038667.pdf
8. Chima, Rodrick V., "*SWIFT Code Assessment for Two Similar Transonic Compressors*", NASA/TM-2009-215520, 2009. Also AIAA Paper 2009-1058. http://ntrs.nasa.gov/archive/nasa/casi.ntrs.nasa.gov/20090011785_2009011333.pdf
9. Veres, J.P., "Axial and Centrifugal Compressor Mean Line Flow Analysis Method", NASA/TM—2009-215585, 2009. Also AIAA Paper 2009–1641. http://ntrs.nasa.gov/archive/nasa/casi.ntrs.nasa.gov/20090042768_2009043888.pdf
10. K. Yamada, K. Funazaki, M. Furukawa, "*The behaviour of tip clearance flow at near-stall condition in a transonic axial compressor rotor*", Proceedings of GT2007 ASME Turbo Expo 2007: Power for Land, Sea and Air, May 14-17, 2007, Montreal, Canada. ASME P.GT2007-27725.
11. K. Yamada, K. Funazaki, and H. Sasaki, "*Numerical investigation of relation between unsteady behaviour of tip leakage vortex and rotating disturbance in a transonic axial compressor rotor*", Proceedings of ASME Turbo Expo 2008: Power for Land, Sea and Air GT2008, June 9-13, 2008, Berlin, Germany. ASME P.GT2008-50779.
12. Shabbir, A., Celestina, M. L., Adamczyk, J. J., and Strazisar, A. J., "*The Effect of Hub Leakage Flow on Two High Speed Axial Compressor Rotors*," ASME Paper 97-GT-346, June, 1997.
13. http://www.cd-adapco.com/products/STAR-CCM_plus/ (retrieved August 6, 2010).
14. Reichardt, H., "*Vollstaendige Darstellung der turbulenten Geschwindigkeitsverteilung in glatten Leitungen*", Z. Angew. Math. Mech, 31(7), pp. 208-219, 1951.
15. Kader, B.A., "*Temperature and Concentration Profiles in Fully Turbulent Boundary Layers*", Int. J. Heat Mass Transfer, 24, pp. 1541-1544, 1981.